



Repositorio Institucional de la Universidad Autónoma de Madrid

<https://repositorio.uam.es>

Esta es la **versión de autor** del artículo publicado en:

This is an **author produced version** of a paper published in:

Applied Catalysis B: Environmental 203 (2017): 166-173

DOI: <http://dx.doi.org/10.1016/j.apcatb.2016.10.015>

Copyright: © 2016 Elsevier

El acceso a la versión del editor puede requerir la suscripción del recurso

Access to the published version may require subscription

Naturally-occurring iron minerals as inexpensive catalysts for CWPO

Macarena Munoz, Patricia Domínguez, Zahara M. de Pedro, Jose A. Casas and Juan J. Rodriguez*

Seccion Departamental Ingenieria Quimica
Universidad Autonoma de Madrid
Crt. Colmenar km 15, 28049 Madrid, Spain

*Corresponding author: Dr. Macarena Munoz

Tel.: +34 91 497 3991

Fax: +34 91 497 3516

E-mail: macarena.munnoz@uam.es

Keywords: CWPO; iron mineral; hematite; magnetite; ilmenite.

Abstract

This work explores the potential application of naturally-occurring minerals as inexpensive catalysts in heterogeneous Fenton, namely catalytic wet peroxide oxidation (CWPO). The availability, low cost and environmentally friendly character of those materials make them interesting candidates for such application. The performance of magnetite, hematite and ilmenite as CWPO catalysts has been tested under different working conditions, which include temperature (25 – 90 °C), H₂O₂ dose (250 – 1000 mg L⁻¹) and catalyst concentration (1 – 4 g L⁻¹). The operating temperature plays a key role on the rate of H₂O₂ decomposition so that with magnetite H₂O₂ conversion after 4 h increased from 8 to 99% by increasing the temperature from 25 to 90 °C. Based on the reaction mechanism proposed, a kinetic model was developed which successfully described the experimental results on H₂O₂ decomposition. The catalytic performance of the minerals tested at temperatures above the ambient was demonstrated using phenol (100 mg L⁻¹) as target pollutant. Unprecedented efficiencies of H₂O₂ consumption, higher than 80% were achieved, allowing high oxidation and mineralization, *i.e.* complete phenol conversion and almost 80% TOC reduction at 75 °C with a catalyst loading of 2 g L⁻¹ and the theoretical stoichiometric amount of H₂O₂ for complete mineralization of phenol (500 mg L⁻¹). Magnetite is particularly attractive, since it showed the highest activity and can be easily separated from the liquid phase given its magnetic properties. All the minerals tested suffered low iron leaching and magnetite and hematite showed a good reusability

upon three consecutive runs. However, in this case long-term durability is not a crucial issue, given the availability and low cost of these minerals.

1. Introduction

Iron minerals are ubiquitous in nature and there is abundant availability of them at minimal cost. Apart from this clear benefit, their environmentally-friendly character as well as their interesting physicochemical properties and relative stability in a wide pH range, make these materials particularly interesting for catalytic wet peroxide oxidation (CWPO), where iron is by far the most commonly used active phase [1].

Main efforts on the field of CWPO are being focused on the development of ferromagnetic catalysts since the recovery and reusability of the catalyst represents a key issue regarding its potential application. Furthermore, due to the presence of both Fe(II) and Fe(III) species they offer a higher ability to promote Fenton-like oxidation than the supported-iron catalysts thus far synthesized [2]. As reported in our recent review [1], magnetic nanoparticles (MNPs) have proved good performance in CWPO and are gaining a growing attention. Although to a lesser extent,

magnetic catalysts prepared by *in-situ* synthesis of magnetite have been also investigated and successfully tested [3, 4]. In particular, hybrid magnetic carbon materials have shown a remarkable performance in CWPO due to their good structural stability and high regeneration and dispersion of the active sites as well as the possibility of tuning the properties of the support [5]. However, the synthesis of MNPs requires dealing with sophisticated methods and complex precursors, which the corresponding economic impact [1]. Moreover, highly efficient separation of the NPs is required, not only for economic reasons but also from environmental considerations since NPs can cause toxic effects in living organisms and act as pollutant carriers. On the other hand, the preparation of conventional magnetic catalysts also involves several steps such as impregnation of a convenient support, usually alumina or activated carbon, with the iron salt and the subsequent thermal treatments (calcination and reduction) to obtain magnetite-based solids [3, 4]. Therefore, the development of inexpensive and sustainable catalysts is a crucial issue regarding potential full-scale application of CWPO in competition with the homogeneous Fenton process of current industrial use (OHP[®], MFC-Foret[®]). In this context, magnetic iron minerals appear as potentially promising catalysts given their huge availability at much lower cost than synthetic materials for this purpose. Nevertheless, so far the experience on the use of iron minerals in CWPO has shown relatively low efficiency of H₂O₂ consumption, slow degradation rates of the organic pollutants and rather low stability due to strong iron leaching under the ambient operating conditions tested [1, 6]. In fact, iron oxides have been proposed essentially as a source of dissolved iron, so that the catalytic action derives in great part from homogenous contribution [7-10]. Testing of these minerals in Fenton-like oxidation has been accompanied in general by the use of large H₂O₂ doses and long reaction times [1]. To overcome those drawbacks, the application of UV or visible irradiation and/or the partial substitution of Fe by other metals such as Co, Cr, Mn, Cu or Ni has been investigated by several authors [6, 11-15]. UV and/or visible irradiation has proved to improve the efficiency by enhancing the production of hydroxyl radicals via decomposition of hydrogen peroxide as well as via photoreduction of Fe(III) to Fe(II) in the mineral surface [6, 16]. On the other hand, although a rather increase of activity has been demonstrated by doping the

minerals with Co [12, 13], Cu [13], Cr [14] and Mn [12, 13], the observed rates are still far from those achieved by the homogeneous Fenton process, and the efficiency of H_2O_2 consumption has not been demonstrated [1].

The main advantage of naturally-occurring iron minerals derives indeed from their direct application without any modification, thus implying a low cost. To achieve this goal, we study in the current work the intensification of the process by increasing the temperature which has been demonstrated to allow a more efficient consumption of H_2O_2 due to enhanced iron-catalyzed H_2O_2 decomposition, improving the oxidation rate and mineralization [17, 18]. The aim of this work is then to optimize the application of natural iron minerals as catalysts in CWPO. Two magnetic minerals, magnetite and ilmenite, and a non-magnetic one, hematite, have been selected for such purpose. They constitute the major iron minerals present in magmatic rocks, which cover most part of the solid earth surface, thus warranting a high availability at low cost [19-21]. The effect of the operating conditions on the decomposition of H_2O_2 promoted by the minerals tested has been evaluated in depth, paying special attention to the effect of temperature. A kinetic model has been accordingly developed to describe the H_2O_2 decomposition. As a case study, the oxidation of phenol, widely used as target compound in oxidation studies, has been investigated focusing on the mineralization yield and the efficiency of H_2O_2 consumption. The stability and reusability of the minerals have been tested in consecutive runs, although this is not a crucial issue, in the particular case of these widely available naturally-occurring inexpensive materials.

2. Materials and methods

2.1. Materials

The natural iron minerals magnetite (Ref. 50121500), hematite (Ref. 50114900) and ilmenite (Ref. 50110700) were provided by Marphil S.L. (Spain). They were sieved into batches of particle diameter <100 μm . Phenol ($\geq 99\%$), hydrogen peroxide solution (30 wt.%) in stable form and nitric acid (65% wt.%) were purchased from Sigma-Aldrich. All the chemicals were used as received without further purification.

2.2. Iron minerals characterization

The composition of the natural iron minerals was determined by total reflection X-ray fluorescence (TXRF) using a TXRF spectrometer 8030c. Their crystalline phases were analyzed by X-ray diffraction (XRD) by a Siemens model D-5000 diffractometer with Cu K α radiation. The porous texture of the fresh and used minerals was characterized from nitrogen adsorption-desorption isotherms at -196 °C using a Micromeritics Tristar 3020 apparatus. The samples were previously outgassed overnight at 150 °C to a residual pressure of 10^{-3} Torr. Elemental analyses were performed in a LECO CHNS-932 Elemental Analyzer. Scanning electron microscopy (SEM) images of the fresh and used iron minerals were obtained using a Philips XL30 microscope. The magnetic characterization of magnetite and ilmenite was carried out using a Quantum Design MPMS XL-5 superconducting quantum interference device (SQUID). The magnetic moment (M) was measured as function of the applied magnetic field (H) at room temperature.

2.3. Typical reaction test

The oxidation experiments were carried out batch-wise in a glass reactor (450 mL), equipped with a PTFE stirrer (700 rpm) and temperature control. The initial pH of the reaction medium was adjusted to 3 with nitric acid solution (1 M) unless otherwise indicated. The catalytic activity of

the natural iron minerals was firstly evaluated in the decomposition of H_2O_2 , analyzing the effect of catalyst ($1\text{--}4\text{ g L}^{-1}$) and H_2O_2 ($250\text{--}1000\text{ mg L}^{-1}$) concentration as well as temperature ($25\text{--}90\text{ }^\circ\text{C}$). Phenol oxidation runs were carried out at $75\text{ }^\circ\text{C}$, 100 mg L^{-1} initial concentration and the theoretical stoichiometric amount of H_2O_2 for complete oxidation of phenol to CO_2 and H_2O (500 mg L^{-1}) with a catalyst load of 2 g L^{-1} . The effect of pH_0 within the range of $3\text{--}7$ was also addressed. Blank experiments in the absence of catalyst were also carried out at each temperature to check the possible contribution of H_2O_2 thermal decomposition. Experiments in the absence of H_2O_2 were carried out as well and negligible adsorption of phenol was observed after 4 h with all the minerals tested.

2.4. Analytical methods

The progress of the reaction was followed by periodically withdrawing samples from the reactor along 4 h. The catalyst was separated by filtration using a PTFE filter (pore size $0.45\text{ }\mu\text{m}$). Phenol was quantified by means of high-performance liquid chromatography (HPLC; Varian Pro-Start 325) using a UV detector and a Microsorb C18 $5\text{ }\mu\text{m}$ column (MV 100, 15 cm length, 4.6 mm diameter) as the stationary phase. The analyses were carried out at 210 nm using sulfuric acid aqueous solution (4 mM) at 1 mL min^{-1} as mobile phase. Total Organic Carbon (TOC) was measured with a TOC analyzer (Shimadzu, mod. TOC, VSCH) and the H_2O_2 concentration was determined by colorimetric titration using the titanium sulfate method [22] with a 1603 Shimadzu UV/Vis spectrophotometer. The Fe leached from the minerals was measured in the reaction effluent by the *o*-phenantroline method [23].

3. Results and discussion

3.1. Iron minerals characterization

The chemical composition, BET surface area and saturation magnetization values (M_s) of the iron minerals are collected in Table 1. The Fe content of hematite, magnetite and ilmenite are very close to the theoretical stoichiometric values of Fe_2O_3 (69.9%), Fe_3O_4 (72.4%) and FeTiO_3 (36.7%), respectively (see Table S1 of the Supplementary Material for transition metal traces present in the minerals). Accordingly, the powder XRD patterns mostly correspond to the standard cards of pure crystalline hematite, magnetite and ilmenite (Figure 1). On the other hand, the measured BET surface area values of the minerals are in good agreement with the previously reported in the literature [8, 12, 24] (see Figure S1 of the Supplementary Material for the N_2 adsorption-desorption isotherms).

Figure 2 shows the magnetization curves of magnetite and ilmenite. The resulting M_s values collected in Table 1 were directly obtained from the magnetization hysteresis loop in the case of magnetite whereas the deduction of the linear component from the sigmoidal function was required for ilmenite (see Figure S2 of the Supplementary Material for details). Notably, despite the significant differences on the magnetic properties of magnetite and ilmenite, both of them could be easily separated from the reaction medium by a magnet.

3.2. Catalytic activity of the iron minerals on the decomposition of H_2O_2

The ability of the natural iron minerals to decompose H_2O_2 was tested within the temperature range of 25 to 90 °C. The effect of catalyst concentration and H_2O_2 dose were previously evaluated (see Figure S3 and S4 of the Supplementary Material for experimental data). The rate of H_2O_2 decomposition increased linearly with the catalyst concentration (1 – 4 g L^{-1}) whereas the H_2O_2 dose (250 – 1000 mg L^{-1}) did not affect to

the rate of decomposition. As can be seen in Figure 3, little, if any, H_2O_2 decomposition occurred at 25 °C (8% at the most, with magnetite). A significant improvement of the decomposition rate of H_2O_2 was clearly observed at increasing temperature. Magnetite yielded higher degradation rates in all cases, allowing complete conversion of H_2O_2 beyond 50 °C. With ilmenite and hematite complete decomposition of H_2O_2 did not occur upon the 4 h time of the experiments. At the highest temperature about 70 and 80% conversion was respectively achieved.

To explain the different performance of the iron minerals several aspects such as Fe content, Fe species, mineral structure, crystallinity and surface reactivity, surface area and reaction mechanism should be taken into account. According to the Fe content, magnetite and hematite should behave similarly whereas ilmenite would give the slowest rate because it contains significantly less Fe (Table 1). Magnetite is a spinel iron oxide containing both Fe(II) and Fe(III) species. Fe(II) occupies the octahedral sites whereas Fe(III) occupies both tetrahedral and octahedral sites [7]. The structure of hematite is based on a hexagonal close-packed oxygen lattice with alternating layers of Fe(III) occupying two thirds of the available octahedra sites [7]. Ilmenite presents a hexagonal structure as well, with two thirds of octahedral positions occupied by cations. Fe(II,III) and Ti(III,IV) are located in alternative layers (Wilson et al., 2005; Raghavender et al., 2013; García-Muñoz et al., 2016) [25]. On the other hand, it should be mentioned that the three minerals showed low BET surface area and a crystalline structure (Table 1 and Figure 1). It is then clear that the main difference between the last two minerals is the kind of iron species. Divalent and trivalent iron are present in ilmenite whereas hematite has only trivalent iron. Therefore, the higher catalytic activity of ilmenite compared to hematite towards H_2O_2 decomposition can be directly related to the presence of both Fe(II) and Fe(III) species in the former. In that sense, magnetite, which showed the highest activity, combines the presence of Fe(II) and Fe(III) in its structure with the highest iron content. Similar conclusions were obtained by Kwan and Voelker (2003)[27] and Matta et al. (2007)[8], who demonstrated that Fe(III) oxides (hematite, goethite, lepidocrocite, ferrihydrite) are less active than their Fe(II) counterparts (magnetite, pyrite) in heterogeneous Fenton oxidation. It should be also considered that the oxidation/reduction reactions on the

mineral surface can lead to the formation of an amorphous precipitate on the surface of the crystalline phase, causing a different kinetic behavior and decomposition rate of H_2O_2 [27], which could vary depending on the mineral tested. To evaluate this, pictures of the minerals surface by scanning electron microscopy (SEM) were taken before and after exposure to H_2O_2 but no significant changes in the surface were found (see Figure S5 of the Supplementary Material for SEM images). Finally, a complete reaction mechanism, explained in detail in the following section, served to describe the decomposition of H_2O_2 in the presence of the three minerals tested. A similar reaction mechanism was reported by Ling and Gurol (1998) [28] for the decomposition of H_2O_2 in the presence of goethite. Those authors also stated that this reaction mechanism can be extrapolated to different iron oxides.

It is important to highlight that iron leaching under the operating conditions tested was practically negligible from ilmenite (2.2 mg L^{-1} at the end of the 4h-experiment, representing 0.02% wt. of the initial content of the mineral) and hematite (1.2 mg L^{-1} , 0.06% wt), and thus, the homogeneous contribution may be neglected. However, the Fe leached to the liquid phase from magnetite was higher, reaching 5.5 mg L^{-1} after the 4 h reaction time. The limited iron leaching of the minerals can be attributed to their crystalline character (See Figure 1). Prucek et al. (2009) [29] investigated the oxidation of phenol using hematites with different crystallinities, concluding that amorphous hematite acts as a homogeneous catalysts due to strong iron leaching upon reaction whereas crystalline hematite served as a heterogeneous catalyst.

3.2.1. Kinetics of H_2O_2 decomposition

The reaction mechanism proposed in this work for the H_2O_2 decomposition promoted by the iron minerals includes the following stages:



The reaction starts with the adsorption of a H_2O_2 molecule onto a free active site (L) of the catalyst [eq. 1]. That molecule is reduced giving rise to a hydroxyl radical, oxidizing the catalyst [eq. 2]. In the next step, a hydroxyl ion is released from the catalyst, becoming the active site positively charged [eq. 3]. The adsorption of a new H_2O_2 molecule reduces the positively-charged active site leading to the formation of a hydroperoxyl radical which remains adsorbed and H^+ , released to the reaction medium [eq. 4]. The radical is finally released and the active site becomes newly available [eq. 5].

The adsorption of the H_2O_2 molecule onto the free active site is assumed the slowest step and thus, the rate-limiting one. Additionally, the concentration of $\text{HOO}\cdot$ is considered constant since it is a reaction intermediate and the steady state condition ($d[\text{HOO}\cdot]/dt = 0$) can be assumed. On the other hand, the concentration of $\text{HO}\cdot$ is proportional to that of H_2O_2 and can be defined as $k\text{C}_{\text{H}_2\text{O}_2}$. Based on these considerations the net decomposition rate of H_2O_2 can be expressed by the following Langmuir-Hinshelwood equation:

$$(-r_{\text{H}_2\text{O}_2}) = - \frac{d\text{C}_{\text{H}_2\text{O}_2}}{dt} = \frac{k_1 \cdot \text{C}_{\text{H}_2\text{O}_2}^2 \cdot \text{C}_{\text{cat}}}{1 + K_2 \cdot \text{C}_{\text{H}_2\text{O}_2}} \quad [6]$$

where $C_{H_2O_2}$ is the concentration of H_2O_2 ; C_{cat} is the catalyst concentration; k_1 is the kinetic constant and K_2 is a lumped parameter, which includes both kinetic and adsorption constants.

Equation 6 was solved by the software package Scientist 3.0 (Micromath[®]). The resulting curves are depicted in Figure 3 together with the experimental values of H_2O_2 concentration at different reaction times. Table 2 collects the values obtained for the rate constants and the correlation coefficients. As observed, the model describes fairly well the time-evolution of H_2O_2 concentration with the three iron minerals within the temperature range investigated except in the case of magnetite at 50 °C. The increase of temperature remarkably favors H_2O_2 decomposition in all cases, although it is particularly important with ilmenite and hematite. Accordingly, the values of apparent activation energy, obtained by fitting those of k_1 to the Arrhenius equation, were significantly higher in the cases of those two minerals (Table 2). Anyway the low values of E_a in all the cases support the assumption of H_2O_2 adsorption being the rate-limiting step. The K_2 values, which includes the equilibrium constant of H_2O_2 adsorption, decreased at increasing temperature.

3.2.2. Activity of the minerals in the CWPO of phenol

As a case study, the catalytic performance of the three iron minerals tested was evaluated in the oxidation of phenol at 75 °C. The effect of pH_0 within 3 -7 was previously investigated but pH_0 3 was selected for further experiments as no improvement on the catalytic activity was observed under circumneutral pH (see Figure S6 of the Supplementary Material for details). The results obtained at pH_0 3 are depicted in Figure 4. As observed, fairly high conversion of H_2O_2 was achieved in all cases but at a moderate rate which favors an efficient consumption of the reagent due to a lower incidence of parasite self-scavenging reactions. That is reflected in the complete conversion of phenol and the fairly high mineralization.

The H₂O₂ efficiency can be defined as the TOC removed per unit of H₂O₂ converted. Unprecedented H₂O₂-efficiency values were achieved (81, 83 and 78% for magnetite, hematite and ilmenite, respectively), well above the reported for homogeneous Fenton oxidation (66%) under similar operating conditions [17]. To discriminate the contribution from the self-decomposition of H₂O₂ with the increase of temperature, a blank experiment in the absence of minerals was conducted under the same operating conditions. It was confirmed that the catalyst plays a key role in the process since in its absence H₂O₂ decomposition was below 5% and TOC removal was almost negligible (<1%) at the end of the 4h-experiment (see Figure S7 of the Supplementary Material for experimental data).

Table 3 collects a literature overview on the application of iron minerals, conventional magnetic catalysts and ferromagnetic nanoparticles in CWPO. As can be seen, most of the works were carried out at ambient temperature using non-feasible amounts of H₂O₂ and/or implying long reaction times. Furthermore, low stability due to strong iron leaching has been commonly found. In fact, iron minerals have been proposed essentially as a source of dissolved iron and chelating agents have been even used to promote the dissolution of iron from the solid [8, 9]. In this sense, the results reported in the current work improve significantly previous ones. It should be also mentioned that those works focused on the disappearance of the target pollutant but further evolution of reaction byproducts or TOC was not followed, which is essential to demonstrate effective degradation. Matta et al. (2007)[8] reported very low conversions (<10%) of 2,4,6-trinitrotoluene (25 mg L⁻¹) after 6 h reaction time using different iron minerals as catalysts (ferrihydrite, hematite, goethite and lepidocrocite (1.76 g L⁻¹)) with extremely high H₂O₂ relative amounts (2.7 g L⁻¹). Magnetite and pyrite led to higher conversion values (85 and 100%, respectively), but accompanied by high iron leaching (14 and 77 mg L⁻¹, respectively) so that homogeneous Fenton oxidation must be the main contribution. In fact, the addition of chelating agents (EDTA, CMCD) to the reaction medium in the presence of magnetite [30] was investigated, leading to an increase on the pollutant conversion from 25 to 60%. In the same line, Xue et al. (2009)[9] required long reaction times (≈9 h) to achieve the complete conversion of pentachlorophenol with magnetite even

using chelating agents to promote the dissolution of iron from the solid. Usman et al. (2012)[10] reported reaction times up to one week for the degradation of oil hydrocarbons with magnetite-rich sandy soil.

The results obtained in the current work are comparable to those achieved with synthetic ferromagnetic catalysts using inert supports [1, 31]. In a former contribution [2], the oxidation of 4-chlorophenol using $\text{Fe}_3\text{O}_4/\gamma\text{-Al}_2\text{O}_3$ was investigated. Up to 80% mineralization was achieved after 4 h reaction time working under similar operating conditions (100 mg L^{-1} 4-chlorophenol, 1 g L^{-1} catalyst, stoichiometric H_2O_2 dose (350 mg L^{-1}), 75°C , pH 3) to those of the current work. On the other hand, natural iron minerals considerably improve the efficiency respect to carbon-supported magnetic catalysts as that support promotes a fast decomposition of H_2O_2 and the recombination of radical species into H_2O and O_2 [3]. The performance of the natural iron minerals is also remarkable compared to the sophisticated magnetic nanoparticles, which have been usually tested with non-feasible H_2O_2 amounts leading to low H_2O_2 consumption efficiency [1, 31, 32].

The oxidation byproducts, not usually considered in the works dealing with the application of iron minerals as Fenton-like catalysts, require special attention since some of them can be significantly more toxic than the starting target pollutants. The oxidation of phenol and phenolic compounds represents a good example in that sense [33-35]. In the current work the main aromatic intermediate detected with the three minerals tested was catechol, appearing also benzoquinone, hydroquinone and resorcinol at significantly lower concentrations. Notably, all of them were degraded at the end of the 4 h-experiment (see Figure S8 of the Supplementary Material for the evolution of aromatic intermediates), being the final reaction products non-toxic short-chain organic acids, mainly oxalic, although formic, acetic, malonic, maleic and fumaric were also detected (see Figure S9 of the Supplementary Material). The color of the reaction medium evolved from colorless to light brown within the first 1-2 h depending on the mineral, giving rise finally to colorless effluents (see Figure S10 of the Supplementary Material). In the cases of magnetite and

hematite the TOC calculated from the identified compounds was above 99% of the directly measured, whereas a difference around 45% was obtained with ilmenite, confirming the lower extension of the reaction in this case leading to non-identified aromatic intermediates and/or condensation by-products in the final effluent [34].

With regard to the potential application of these minerals as catalysts it is interesting to learn on the possible leaching of iron under the operating conditions. The concentration of dissolved iron in the liquid phase at the end of 4 h-experiment was 13, 3 and 1 mg L⁻¹ with magnetite, hematite and ilmenite, respectively, representing as less as 1.8, 0.5 and 0.3% of their initial iron-content. It should be also mentioned that the leaching of Ti from ilmenite was negligible as well (<0.1%). Nevertheless, it is important to highlight that those concentrations were directly related to the amount of oxalic acid formed upon reaction. In this sense, during the first 1-2 h of reaction (depending on the mineral used, Figure S9 of the Supplementary Material) the concentration of leached Fe was negligible (<0.2 mg L⁻¹) and thus, the mineralization and complete degradation of phenol, which occurred mostly within that time, can be attributed to the CWPO promoted by the minerals. The evolution of leached Fe is depicted in Figure S11 of the Supplementary Material.

3.2.3. Reusability tests

To learn more on the catalytic performance of the minerals, three successive experiments were carried out with each of them. The catalyst was simply dried overnight at low temperature (60 °C) after each run. The results in terms of phenol conversion, TOC reduction, H₂O₂ decomposition and Fe leached are collected in Figure 5.

Although magnetite suffered the highest iron leaching it was also the mineral showing the best performance upon the three sequential runs, maintaining or even slightly increasing the percentage of mineralization. These results were consistent with the amount of Fe leached, which decreased along the three successive runs. In the first one, the homogeneous Fenton contribution must be important given the iron concentration in the liquid phase. That increases the rate of hydroxyl radical generation which affects negatively to the efficiency of the process favoring self-scavenging reactions. In subsequent runs, where iron leaching was lower, the homogeneous contribution was less and less important, and a slight improvement of mineralization was observed. Hematite yielded slight decreases of mineralization upon the three sequential runs whereas ilmenite, unexpectedly, was strongly deactivated, showing negligible activity upon the second and third runs.

The magnetic properties of magnetite and ilmenite remained unchanged after their sequential application (see Figure S12 in Supplementary Material for magnetization hysteresis loops), thus warranting the easy separation of the solid after the treatment. The composition of the iron minerals did not suffer any significant change after their successive use in CWPO. Elemental analyses of the used minerals allowed discarding the presence of carbonaceous deposits since the carbon content remained almost negligible in all cases (magnetite: 0.36% (fresh: 0.39%); hematite: 0.07% (fresh: 0.09%); ilmenite: 0.06% (fresh: 0.09%)). Accordingly, their BET surface areas did not decrease upon use (10, 9 and 4 m² g⁻¹ for hematite, magnetite and ilmenite, respectively). In the same line, the structure of the minerals remained unchanged for magnetite and hematite (see Figure S13 and S14 of the Supplementary Material for XRD patterns of magnetite and hematite after being used in reaction, respectively) whereas some changes, mainly the appearance of higher peaks corresponding to hematite phases (e.g. at $2\theta = 24.2^\circ$ and 24.6°), were found in the used ilmenite, as can be observed in Figure 6. Passivation of the surface of the mineral and, thus, oxidation of Fe(II) to Fe(III), seems to occur during the reaction, leading to the aforementioned almost complete deactivation of ilmenite. This finding is consistent with the progressive passivation of the ilmenite surface upon photocatalytic oxidation of phenol with H₂O₂ recently reported in the literature [16].

The good reusability shown by magnetite under the operating conditions is comparable to that of $\text{Fe}_3\text{O}_4/\gamma\text{-Al}_2\text{O}_3$ catalysts, whose activity remained unchanged after three sequential runs in chlorophenol oxidation [2]. That behavior was better than the reported by Nguyen et al. (2011) [3] for an activated carbon-supported magnetic catalyst which gave higher Fe leaching (Table 3). On the other hand, the results obtained with magnetite at 75 °C substantially improve those reported with different iron minerals under ambient conditions [2, 36, 37]. Liang et al. (2010) [37] investigated the decoloration of acid orange II (70 mg L^{-1}) by natural vanadium-titanium magnetite (1 g L^{-1}) with 340 mg L^{-1} of H_2O_2 at 35 °C. They observed a decrease on the pollutant conversion from 98 (1st run) to 90% (3rd run), which was attributed to iron leaching. Nguyen et al. (2011)[3] used a catalyst based on Fe_3O_4 over activated carbon (2.5 g L^{-1}) in the oxidation of methyl orange (50 mg L^{-1}) under ambient conditions. The conversion of the target pollutant decreased from 100 to 85% after three sequential runs, also associated to iron leaching. Similarly, the performance of the magnetite mineral compares favorably with that of ferromagnetic nanoparticles [31, 38, 39], whose stability was negatively affected by a number of shortcomings like aggregation, iron leaching and nanoparticles loss during supernatant discharge (Table 3). E.g. Xu et al. (2012) [39] applied colloidal ferromagnetic nanoparticles in the oxidation of 2,4-dichlorophenol and observed a decrease on the activity around 60% after five consecutive runs.

4. Conclusions

In this work, it has been demonstrated that iron minerals can act as efficient CWPO catalysts working at temperatures well above the ambient. The enhanced performance of the minerals was confirmed in the CWPO of phenol at 75 °C, allowing the complete conversion of the target pollutant with a high mineralization (70-80%). The H_2O_2 efficiency was remarkably higher than the observed in the homogeneous Fenton under

similar operating conditions and comparable to the obtained with synthetic ferromagnetic catalysts. Since the conventional homogeneous Fenton process is currently used at industrial scale (OHP®, MFC-Foret®) at temperatures well above the ambient, inexpensive naturally-occurring iron minerals could be used replacing iron salts in such applications. With regard to the thermal requirements, it has to be considered that heat can be recovered from the exit stream and the exothermic character of the oxidation process provides also an enthalpy source. Although the stability of the minerals is not a critical issue given their high availability and low cost, it has been also demonstrated that their reusability (magnetite and hematite) is comparable to that showed by synthetic supported iron catalysts and better than the exhibited by the widely investigated ferromagnetic nanoparticles. Naturally-occurring magnetite appears particularly promising among the three minerals tested due to its high activity, outstanding reusability and easy magnetic separation from the liquid phase.

Acknowledgments

This research has been supported by the Spanish MINECO through the project CTQ2013-4196-R and by the CM through the project S2013/MAE-2716. M. Munoz thanks the Spanish MINECO for a Juan de la Cierva-Incorporación postdoctoral contract (IJCI-2014-19427).

Figure and Table Captions

Table 1. Characterization of the natural iron minerals tested.

Table 2. Values of the rate constants (k_1 : $\text{L}^2 \text{mg}^{-1} \text{min}^{-1} \text{g}_{\text{cat}}^{-1}$; K_2 : L mg^{-1}) and activation energies (kJ mol^{-1}) ($[\text{H}_2\text{O}_2]_0 = 500 \text{ mg L}^{-1}$; $[\text{magnetite}] = 1 \text{ g L}^{-1}$; $[\text{hematite}] = [\text{ilmenite}] = 2 \text{ g L}^{-1}$; $\text{pH}_0 = 3$).

Table 3. Summary of the studies devoted to the application of natural iron minerals, conventional magnetic catalysts and ferromagnetic nanoparticles as catalysts in Fenton oxidation.

Figure 1. XRD patterns of hematite (a), magnetite (b) and ilmenite (c). Major peaks are identified using ICDD PDF 98-001-5840 (Fe_2O_3), 98-016-4813 (Fe_3O_4) and 98-000-9805 (FeTiO_3).

Figure 2. Magnetization hysteresis loops of magnetite (a) and ilmenite (b). The inset shows a photograph of magnetite (left) and ilmenite (right) in water under a magnetic field.

Figure 3. H_2O_2 decomposition promoted by magnetite (a), ilmenite (b) and hematite (c) ($[\text{H}_2\text{O}_2]_0 = 500 \text{ mg L}^{-1}$; $[\text{magnetite}] = 1 \text{ g L}^{-1}$; $[\text{hematite}] = [\text{ilmenite}] = 2 \text{ g L}^{-1}$; $\text{pH}_0 = 3$). Experimental data (symbols) and predicted values obtained from the kinetic model (solid lines).

Figure 4. Time-course of phenol, TOC and H_2O_2 upon CWPO with the minerals tested ($T = 75 \text{ }^\circ\text{C}$; $\text{pH}_0 = 3$; $[\text{Phenol}]_0 = 100 \text{ mg L}^{-1}$; $[\text{H}_2\text{O}_2]_0 = 500 \text{ mg L}^{-1}$; $[\text{mineral}] = 2 \text{ g L}^{-1}$).

Figure 5. Phenol conversion, TOC reduction (both bars) H_2O_2 decomposition and Fe leached (both symbols) upon CWPO of phenol with the minerals tested in three successive applications ($[\text{Phenol}]_0 = 100 \text{ mg L}^{-1}$; $[\text{H}_2\text{O}_2]_0 = 500 \text{ mg L}^{-1}$; $[\text{mineral}] = 2 \text{ g L}^{-1}$; $\text{pH}_0 = 3$; $T = 75 \text{ }^\circ\text{C}$; $t = 4 \text{ h}$).

Figure 6. XRD patterns of ilmenite before (a) and after being used in the CWPO of phenol upon three sequential runs (b).

References

- [1] M. Munoz, Z.M. de Pedro, J.A. Casas, J.J. Rodriguez, Appl. Catal., B 176-177 (2015) 249–265.
- [2] M. Munoz, Z.M. de Pedro, J.A. Casas, J.J. Rodriguez, Chem. Eng. J. 228 (2013) 646–654.
- [3] T.D. Nguyen, N.H. Phan, M.H. Do, K.T. Ngo, J. Hazard. Mater. 185 (2011) 653–661.
- [4] M. Munoz, Z.M. de Pedro, N. Menendez, J.A. Casas, J.J. Rodriguez, Appl. Catal., B 136-137 (2013) 218–224.
- [5] R.S. Ribeiro, A.M.T. Silva, J.L. Figueiredo, J.L. Faria, H.T. Gomes, Appl. Catal., B 187(2016) 428–460.
- [6] P.V. Nidheesh, RSC Adv. 5 (2015) 40552–40577.
- [7] M.C. Pereira, L.C.A. Oliveira, E. Murad, Clay Miner. 47 (2012) 285–302.
- [8] R. Matta, K. Hanna, S. Chiron, Sci. Total Environ. 385 (2007) 242–251.
- [9] X. Xue, K. Hanna, C. Despas, F. Wu, N. Deng, J. Mol. Catal. A: Chem 311 (2009) 29–35.
- [10] M. Usman, P. Faure, K. Hanna, M. Abdelmoula, C. Ruby, Fuel 96 (2012) 270–276.
- [11] Y. Zhong, X. Liang, Z. He, W. Tan, J. Zhu, P. Yuan, R. Zhu, H. He, Appl. Catal., B 150-151 (2014) 612–618.
- [12] R.C.C. Costa, M.F.F. Lelis, L.C.A. Oliveira, J.D. Fabris, J.D. Ardisson, R.R.V.A. Rios, C.N. Silva, R.M. Lago, J. Hazard. Mater. 129 (2006) 171–178.
- [13] P. Baldrian, V. Merhautová, J. Gabriel, F. Nerud, P. Stopka, M. Hrubý, M.J. Benes, Appl. Catal., B 66 (2006) 258–264.
- [14] F. Magalhaes, M.C. Pereira, S.E.C. Botrel, J.D. Fabris, W.A. Macedo, R. Mendoça, R.M. Lago, L.C.A. Oliveira, Appl. Catal., A 332 (2007) 115–123.

- [15] X. Liang, Z. He, G. Wei, P. Liu, Y. Zhong, W. Tan, P. Du, J. Zhu, H. He, J. Zhang, *J. Colloid Interface Sci.* 426 (2014) 181–189.
- [16] P. García-Muñoz, G. Pliego, J.A. Zazo, a. Bahamonde, J.A. Casas, *J. Environ. Chem. Eng.* 4 (2016) 542–548.
- [17] J.A. Zazo, G. Pliego, S. Blasco, J.A. Casas, J.J. Rodriguez, *Ind. Eng. Chem. Res.* 50 (2011) 866–870.
- [18] G. Pliego, J.A. Zazo, S. Blasco, J.A. Casas, J.J. Rodriguez, *Ind. Eng. Chem. Res.* 51 (2012) 2888–2896.
- [19] H. He, Y. Zhong, X. Liang, W. Tan, J. Zhu, C. Yan Wang, *Nature Scientific Reports* 5 (2015) 1–10.
- [20] B.R. Frost, *Rev. Mineral. Geochem.* 25 (1991) 489–509.
- [21] B.R. Frost and D.H. Lindsley, *Rev. Mineral. Geochem.* 25 (1991) 433–468.
- [22] G.M. Eisenberg, *Ind. Eng. Chem. Res.* 15 (1943) 327–328.
- [23] E.B. Sandell, *Colorimetric determination of traces of metals*, Interscience Pubs., New York, (1959).
- [24] T. Tao, Y. Chen, D. Zhou, H. Zhang, S. Liu, R. Amal, N. Sharma, A.M. Glushenkov, *Chem. Eur. J.* 19 (2013) 1091–1096.
- [25] N.C. Wilson, J. Muscat, D. Mkhonto, P.E. Ngoepe, N.M. Harrison, *Phys. Rev. B* 71 (2005) 075202-1–075202-9.
- [26] A.T. Raghavender, N.H. Hong, K.J. Lee, M.H. Jung, Z. Skoko, M. Vasilevskiy, M.F. Cerqueira, A.P. Samantilleke, *J. Magn. Magn. Mater.* 331 (2013) 129-132.
- [27] W.P. Kwan, B.M. Voelker, *Environ. Sci. Technol.* 37 (2003) 1150–1158.
- [28] S.S. Ling, M.D. Gurol, *Environ. Sci. Technol.* 32 (1998) 1417–1423.
- [29] R. Prucek, M. Hermanek, R. Zboril, *Appl. Catal., A* 366 (2009) 325–332.
- [30] R. Matta, K. Hanna, T. Kone, S. Chiron, *Chem. Eng. J.* 144 (2008) 453–458.

- [31] J. Zhang, J. Zhuang, L. Gao, Y. Zhang, N. Gu, J. Feng, D. Yang, J. Zhu, X. Yan, *Chemosphere* 73 (2008) 1524–1528.
- [32] S. Zhang, X. Zhao, H. Niu, Y. Shi, Y. Cai, G. Jiang, *J. Hazard. Mater.* 167 (2009) 560–566.
- [33] J.A. Zazo, J.A. Casas, C.B. Molina, A. Quintanilla, J.J. Rodriguez, *Environ. Sci. Technol.* 41 (2007) 7164–7170.
- [34] M. Munoz, Z.M. de Pedro, J.A. Casas, J.J. Rodriguez, *J. Hazard. Mater.* 190 (2011) 993–1000.
- [35] M. Munoz, Z.M. de Pedro, G. Pliego, J.A. Casas, J.J. Rodriguez, *Ind. Eng. Chem. Res* 51 (2012) 13092–13099.
- [36] Y. Zhong, X. Liang, Y. Zhong, J. Zhu, S. Zhu, P. Yuan, H. He, J. Zhang, *Water Res.* 46 (2012) 4633–4644.
- [37] X. Liang, Y. Zhong, S. Zhu, J. Zhu, P. Yuan, H. He, J. Zhang, *J. Hazard. Mater.* 181 (2010) 112–120.
- [38] K. Rusevova, F. Kopinke, A. Georgi, *J. Hazard. Mater.* 241–242 (2012) 433–440.
- [39] L. Xu, J. Wang, *Appl. Catal., B* 123–124 (2012) 117–126.
- [40] S. Xavier, R. Gandhimathi, P.V. Nidheesh, S.T. Ramesh, *Desalin. Water Treat.* 53 (2015) 109–118.
- [41] H.S. Oliveira, L.D. Almeida, V.A.A. de Freitas, F.C.C. Moura, P.P. Souza, L.C.A. Oliveira, *Catal. Today* 240 (2015) 176–181.
- [43] W. Guanghua, W. Dong, L. Wenbing, L. Yunzhou, C. Kun, *Chin. J. Env. Eng.* 8 (2014) 1857–1862.

Table 1

Natural iron mineral	Fe (%)	Ti (%)	S_{BET} ($\text{m}^2 \text{g}^{-1}$)	M_s (emu g^{-1})
Hematite (Fe_2O_3)	61.4	--	9	--
Magnetite (Fe_3O_4)	73.0	--	8	77.7
Ilmenite (FeTiO_3)	36.2	37.0	4	0.19

Table 2

Temperature ($^{\circ}\text{C}$)	Magnetite (Fe_3O_4)			Ilmenite (FeTiO_3)			Hematite (Fe_2O_3)		
	$k_1 \times 10^3$	K_2	r^2	$k_1 \times 10^3$	K_2	r^2	$k_1 \times 10^3$	K_2	r^2
25	1.01	3.00	0.999	--	--	--	--	--	--
50	9.04	1.11	0.993	1.09	1.90	0.999	0.93	2.25	0.999
75	11.0	1.02	0.999	2.18	1.28	0.999	2.44	1.29	0.999
90	13.3	0.71	0.999	4.67	0.90	0.976	3.14	1.13	0.999
Ea	9.2		0.986	34.2		0.980	30.5		0.989

Table 3

Iron minerals							
Catalyst	Operating conditions				Results	Stability	Reference
	T (°C)	pH	Target pollutant	H ₂ O ₂ dose and catalyst concentration			
Ferrihydrite, hematite, goethite, lepidocrocite, magnetite, pyrite	20-25	3	2,4,6-trinitrotoluene (25 mg L ⁻¹)	[H ₂ O ₂] ₀ = 2.7 g L ⁻¹ [catalyst] = 1.76 g L ⁻¹	X _{cont} < 10% (ferrihydrite, hematite, goethite, lepidocrocite) X _{cont} = 85% (magnetite) X _{cont} = 100% (pyrite) (reaction time = 6 h)	Iron leaching : -Ferrihydrite, hematite, goethite and lepidocrocite: 1 µg L ⁻¹ -Magnetite: 14 mg L ⁻¹ -Pyrite: 77 mg L ⁻¹	Matta et al. (2007) [8]
Magnetite		7	Pentachlorophenol (50 mg L ⁻¹)	[H ₂ O ₂] ₀ = 5 g L ⁻¹ [catalyst] = 2.0 g L ⁻¹	X _{cont} = 90% (reaction time = 9 h)	Iron leaching : 14 mg L ⁻¹	Xue et al. (2009) [9]
Vanadium-titanium magnetite		3	Acid Orange II (50 mg L ⁻¹)	[H ₂ O ₂] ₀ = 0.34 g L ⁻¹ [catalyst] = 1.0 g L ⁻¹	X _{cont} = 98% (reaction time = 4 h)	3 runs X _{cont-3rd} = 90%	Liang et al. (2010) [37]
Magnetite rich sandy		6.7	Oil hydrocarbon (40 mg L ⁻¹)	[H ₂ O ₂] ₀ = 10 g L ⁻¹ [catalyst] = 100 g L ⁻¹	X _{cont} > 80% (reaction time = one week)	Not evaluated	Usman et al. (2012) [10]

Magnetite		2	Magenta MB (50 mg L ⁻¹)	[H ₂ O ₂] ₀ = 8.8 g L ⁻¹ [catalyst] = 0.6 g L ⁻¹	X _{cont} = 87% (reaction time = 1 h)	Not evaluated	Xavier et al. (2015) [40]
Nb-doped hematite		5.5	Methylene blue (10 mg L ⁻¹)	[H ₂ O ₂] ₀ = 272 g L ⁻¹ [catalyst] = 10 g L ⁻¹	X _{cont} = 75% (reaction time = 2 h)	5 runs X _{cont-5th} = 60%	Oliveira et al. (2015) [41]
Ilmenite		3	Phenol (100 mg L ⁻¹)	[H ₂ O ₂] ₀ = 0.5 g L ⁻¹ [catalyst] = 0.45 g L ⁻¹	X _{cont} = 100% X _{TOC} = 50% (reaction time = 8 h)	Iron leaching : 2.3 mg L ⁻¹	Garcia-Muñoz et al. (2016) [16]
Magnetite, ilmenite, hematite	75	3	Phenol (100 mg L ⁻¹)	[H ₂ O ₂] ₀ = 0.5 g L ⁻¹ [catalyst] = 2 g L ⁻¹	X _{cont} = 100% X _{TOC} ~ 70% (reaction time = 4 h)	3 runs X _{TOC-3rd} = 77% (magnetite) X _{TOC-3rd} = 69% (hematite) X _{TOC-3rd} = 1% (ilmenite)	This work
Conventional ferromagnetic catalysts							
Magnetic Fe ₂ MO ₄ activated carbon	30	4	Methyl orange (50 mg L ⁻¹)	[H ₂ O ₂] ₀ = 0.6 g L ⁻¹ [catalyst] = 2.5 g L ⁻¹	X _{cont} = 100% X _{TOC} = 59% (reaction time = 2 h)	3 runs X _{cont-3rd} = 85%	Nguyen et al. (2011) [3]
Magnetic	70	3	4-chlorophenol (100 mg L ⁻¹)	[H ₂ O ₂] ₀ = 0.35 g L ⁻¹	X _{cont} = 100%	3 runs	Munoz et al.

Fe ₃ O ₄ /γ-Al ₂ O ₃			L ⁻¹)	[catalyst] = 1.0 g L ⁻¹	X _{TOC} = 84% (reaction time = 4 h)	X _{cont-3rd} = 100% X _{TOC-3rd} = 78%	al. (2013) [1]
Magnetic bentonite	40	3	Orange II (175 mg L ⁻¹)	[H ₂ O ₂] ₀ = 0.71 g L ⁻¹ [catalyst] = 0.6 g L ⁻¹	X _{cont} = 100% (reaction time = 3 h)	4 runs X _{cont-4th} = 100%	Gua ngh ua et al. (2014) [43]
Ferromagnetic nanoparticles							
Magnetic nanoparticles	35	7	Phenol (94 mg L ⁻¹)	[H ₂ O ₂] ₀ = 40 g L ⁻¹ [catalyst] = 5.0 g L ⁻¹	X _{cont} = 100% X _{TOC} = 43% (reaction time = 6 h)	8 runs X _{cont-8th} = 80% X _{TOC-8th} = 30%	Zha ng et al. (2009) [32]
Magnetic nanoparticles	22	7	Phenol (25 mg L ⁻¹)	[H ₂ O ₂] ₀ = 5.0 g L ⁻¹ [catalyst] = 3.0 g L ⁻¹	X _{cont} = 60% (reaction time = 24 h)	3 runs X _{cont-3rd} = 30%	Rus evov a et al. (2012) [38]
Magnetic nanoparticles	30	3	2,4-dichlorophenol (100 mg L ⁻¹)	[H ₂ O ₂] ₀ = 0.4 g L ⁻¹ [catalyst] = 1.0 g L ⁻¹	X _{cont} = 100% X _{TOC} = 51%	5 runs X _{cont-5th} = 40%	Xu and Wan

					(reaction time = 3 h)		g (201 2) [39]
--	--	--	--	--	-----------------------	--	-------------------------

Figure 1

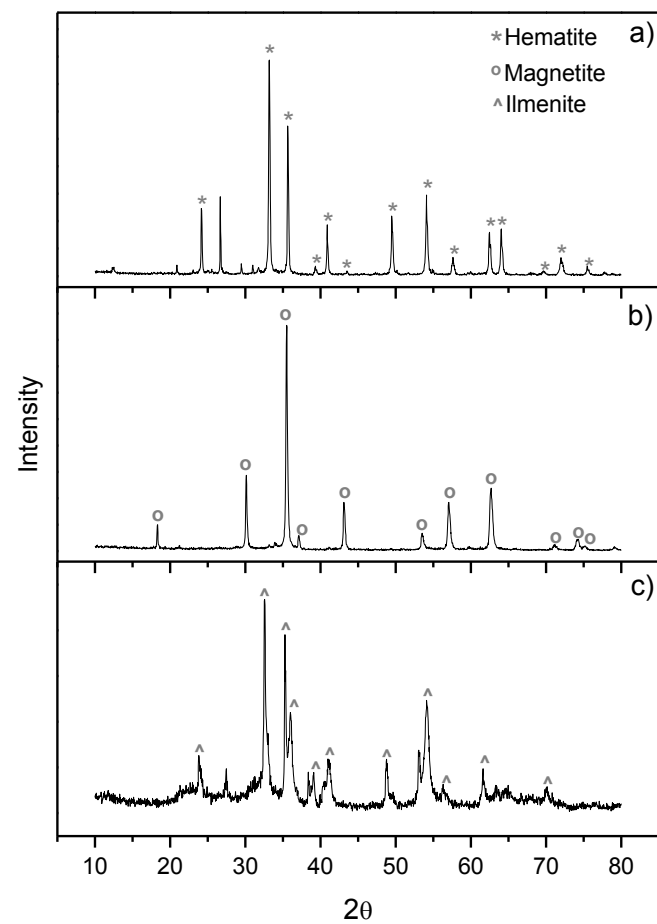


Figure 2

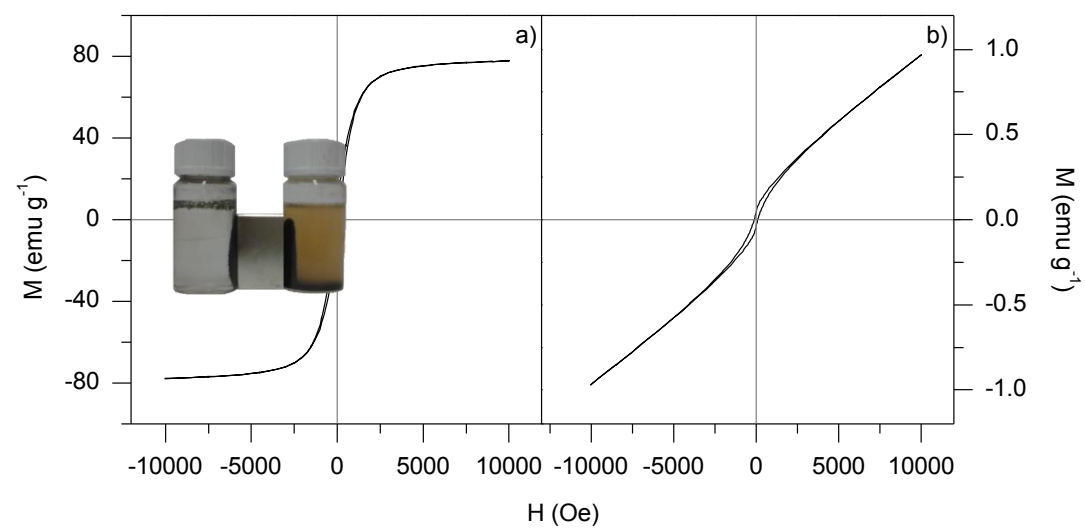


Figure 3

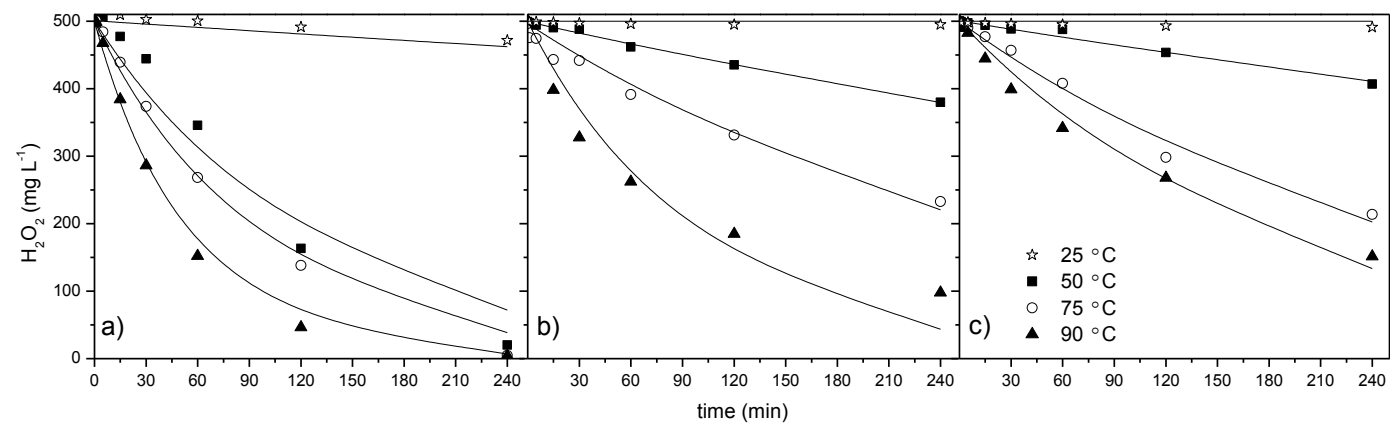


Figure 4

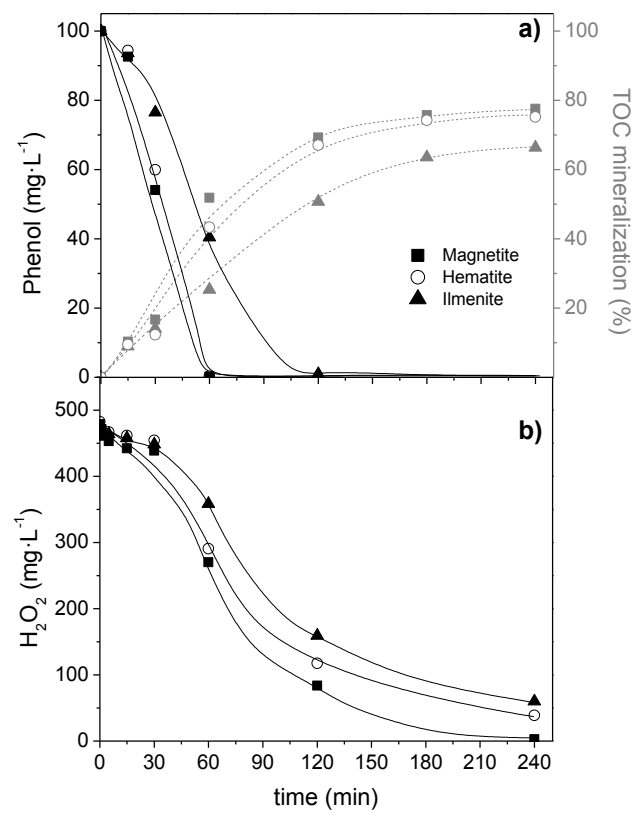


Figure 5

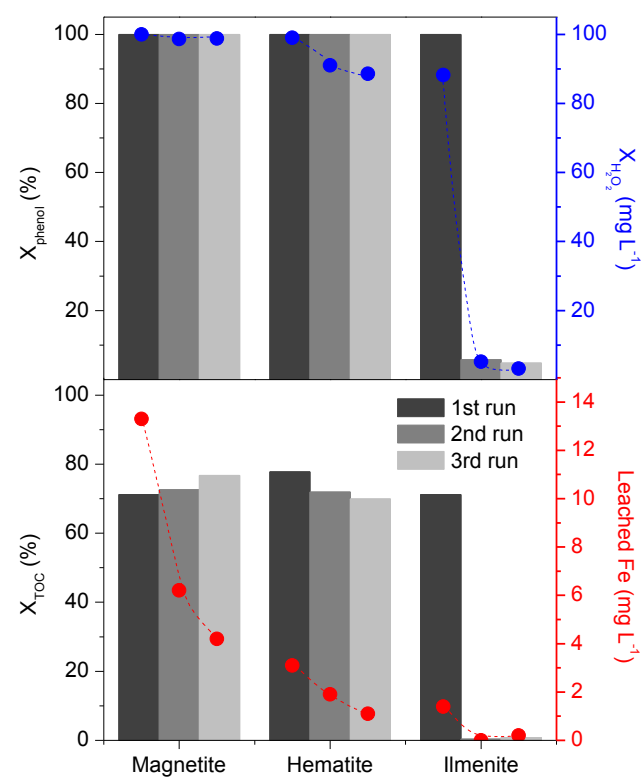


Figure 6

